

UNIAXIAL COMPRESSION TEST AND STRESS WAVE PROPAGATION MODELLING USING SPH

Rajarshi DAS and Paul W. CLEARY

CSIRO Mathematical and Information Sciences, Clayton, Victoria 3168, AUSTRALIA

ABSTRACT

The paper demonstrates the application of Smoothed Particle Hydrodynamics (SPH) for modelling compression and stress wave propagation in elastic solids. This is illustrated using a laboratory scale uniaxial compression test under different loading conditions. To validate the SPH based approach, the results are compared to matching results using the Finite Element Method. The solutions predicted by Smoothed Particle Hydrodynamics are found to agree well. This paper illustrates the potential of Smoothed Particle Hydrodynamics for accurate and efficient modelling of solid materials that are subjected to compression, and of the resulting elastic wave propagation.

INTRODUCTION

The uniaxial test is the most widely used mechanical testing process for characterising solid material behaviour. It is a simple and versatile method for determining material properties in almost all kinds of material applications (Bradley *et al.*, 2001). Uniaxial tests are also employed to study localised deformation behaviour, such as strain distribution around a notch in a specimen (Nawrocki *et al.*, 1998). In this test, a standard specimen is gripped between the jaws of a tensile testing machine. One end of the specimen is pushed/pulled by a moving piston and the other end is held under a fixed jaw. The compression or elongation in the specimen is measured by extensometers.

Computational modelling offers an improved way of understanding the deformation behaviour, which in turn can assist in determining the test parameters (Li and Wang, 2004). For example, in the case of a planar tension test, the specimen must be in plain strain condition during deformation. This is ensured by a specimen of high aspect ratio and wide jaw grips to prevent lateral contraction. A priori modelling of the test can help design the optimum specimen dimensions and type of apparatus to be used to ensure a plain strain condition. Modelling can also be used to guide the instrumentation process. An initial analysis can determine the areas of large strains in flexible materials, hence can warrant locations of measurement and type of instrumentations required. For example, video extensometry technique is useful for measuring large strains and capturing necking processes (instead of using conventional mechanical extensometers). In this work we use a mesh-free method Smoothed Particle Hydrodynamics (SPH) (Monaghan, 1992) to model uniaxial testing of laboratory scale specimens.

Numerical modelling of fracture with traditional mesh-based techniques (e.g. FEM and BEM) requires a very fine mesh to model the theoretically singular stress field in the neighbourhood of damage locations (e.g. crack tip). One common approach to simulate crack propagation with FEM is to release the adjacent nodes of the elements representing damaged areas (Aliabadi and Rooke, 1991). Furthermore, as the damage evolves, the structure needs to be re-meshed to take into account the localised change in geometry. Automated re-meshing can lead to mesh distortion and inaccurate results, especially in gradient computations (Fernandez-Mendez *et al.*, 2005). Due to the mesh-free nature of SPH, the fracturing process and the associated change in structural configuration can be easily handled without the need to re-mesh.

SPH uses a particle based Lagrangian approach, in which the frame of reference is attached to the moving particles. This gives the ability to track history dependent properties of the material (Cleary *et al.*, 2005). In general a fracturing process is driven by the stress-strain history in the material. Traditional Eulerian methods experience difficulties in capturing the stress-strain history on a particle by particle basis and predicting the evolution of damage in the specimen. The history tracking ability of SPH can be utilised to monitor the damage initiation and crack propagation, thus providing failure history of the specimen. The dynamics of damage evolution can thus be explicitly included in the analysis.

The SPH method has been successfully applied to model different types of metal forming processes involving large deformation (Cleary *et al.*, 2006). In this work, the aim is to establish SPH as an effective and accurate computational method to predict transient stress field in an elastic solid, which can then be extended to model brittle fracture under compressive loads. In the initial transient state of uniaxial compressive loading, the elastic stress wave propagation through the specimen affects its response. It is important to analyse transient structural behaviour in that the initial fluctuating stress field can trigger generation and propagation of localised damages/flaws, which can then play a critical role in initiating the fracture failure of the specimen. The stress wave generation and propagation through the specimen as a result of contact excitation by a piston is therefore investigated. The ability of SPH to model stress waves is illustrated using a simple problem of modelling a uniaxial tester. We also use the fundamentally different and widely used Finite Element Method for modelling the same example so as to compare and correlate the FE results with the SPH solutions.

SMOOTHED PARTICLE HYDRODYNAMICS (SPH) METHOD

A brief summary of the SPH method is presented here. SPH has been extended to modelling of a variety of solid deformation problems (Libersky and Petschek, 1990, Wingate and Fisher, 1993, Gray *et al.*, 2001, and more recently by Cleary *et al.*, 2006). The interpolated value of a function A at any position \mathbf{r} can be expressed using SPH smoothing as:

$$A(\mathbf{r}) = \sum_b m_b \frac{A_b}{\rho_b} W(\mathbf{r} - \mathbf{r}_b, h) \quad (1)$$

where m_b and \mathbf{r}_b are the mass and the density of particle b and the sum is over all particles b within a radius $2h$ of \mathbf{r} . Here $W(\mathbf{r}, h)$ is a C^2 spline based interpolation or smoothing kernel with radius $2h$, that approximates the shape of a Gaussian function, but has compact support. The gradient of the function A is given by differentiating the interpolation equation (1) to give:

$$\nabla A(\mathbf{r}) = \sum_b m_b \frac{A_b}{\rho_b} \nabla W(\mathbf{r} - \mathbf{r}_b, h) \quad (2)$$

Using these interpolation formulae and suitable finite difference approximations for second order derivatives, one is able to convert parabolic partial differential equations into ordinary differential equations for the motion of the particles and the rates of change of their properties. We now present the differential equations governing the structural responses and their SPH approximations.

Continuity Equation

From Monaghan (1992), our preferred form of the SPH continuity equation is:

$$\frac{d\rho_a}{dt} = \sum_b m_b (\mathbf{v}_a - \mathbf{v}_b) \cdot \nabla W_{ab} \quad (3)$$

where ρ_a is the density of particle a with velocity \mathbf{v}_a and m_b is the mass of particle b . We denote the position vector from particle b to particle a by $\mathbf{r}_{ab} = \mathbf{r}_a - \mathbf{r}_b$, and let $W_{ab} = W(\mathbf{r}_{ab}, h)$ be the interpolation kernel with smoothing length h evaluated for the distance $|\mathbf{r}_{ab}|$. This form of the continuity equation is Galilean invariant (since the positions and velocities appear only as differences), has good numerical conservation properties, and is not affected by density discontinuities or free surfaces.

Momentum Equation

The SPH momentum equation used for the elasto-plastic deformation of the solids is:

$$\frac{dv^i}{dt} = \frac{1}{\rho_s} \frac{\partial \sigma^{ij}}{\partial x^j} + g^i \quad (4)$$

where v is the velocity, g denotes the body force, and σ is the stress tensor which can be written as:

$$\sigma^{ij} = -P_s \delta^{ij} + S^{ij} \quad (5)$$

where P_s is the pressure and S is the deviatoric stress. Assuming Hooke's law with shear modulus μ_s , the evolution equation for the deviatoric stress S (Gray *et al.*, 2001) is:

$$\frac{dS^{ij}}{dt} = 2\mu_s \left(\dot{\epsilon}^{ij} - \frac{1}{3} \delta^{ij} \dot{\epsilon}^k{}^k \right) + S^{ik} \Omega^{jk} + \Omega^{ik} S^{kj} \quad (6)$$

where

$$\dot{\epsilon}^{ij} = \frac{1}{2} \left(\frac{\partial v^i}{\partial x^j} + \frac{\partial v^j}{\partial x^i} \right) \quad (7)$$

and

$$\Omega^{ij} = \frac{1}{2} \left(\frac{\partial v^i}{\partial x^j} - \frac{\partial v^j}{\partial x^i} \right) \quad (8)$$

is the rotation tensor. The following equation of state is used:

$$P_s = c_0^2 (\rho_s - \rho_{s0}) \quad (9)$$

where ρ_{s0} is the reference density. The subscript s in the above symbols refers to the solid state. The bulk modulus is $K = \bar{\rho}_s c_0^2$ and the Poisson ratio ν_s is:

$$\nu_s = \frac{(3K/\mu_s - 2)}{2(3K/\mu_s + 2)} \quad (10)$$

TEST CONFIGURATION SPECIFICATION

The uniaxial tester is modelled with SPH via an axially loaded rectangular specimen of width 86 mm and height 140 mm, as shown in Figure 1. The specimen is made of an elastic material of bulk modulus of 12.2 GPa, shear modulus of 2.67 GPa and density of 2300 kg/m³. It is held fixed at the bottom by a rigid plate, and the load is applied through a piston on the top, see Figure 1. This simulates the requisite boundary conditions for a typical uniaxial compression test.

The stress wave propagation in the specimen was analysed using Smoothed Particle Hydrodynamics (SPH). The specimen domain was discretised with particles of resolution 1 mm, giving a total of 12,040 particles in the two dimensional simulation. The partial differential equations governing the stress and displacement fields in elastic solids (Equations 1-10) were used to evaluate the structural response. A cubic kernel interpolation function was used for this problem. Based on the material properties, the time step was 0.261 μ s. An Improved Euler explicit integration scheme was used for the time stepping.

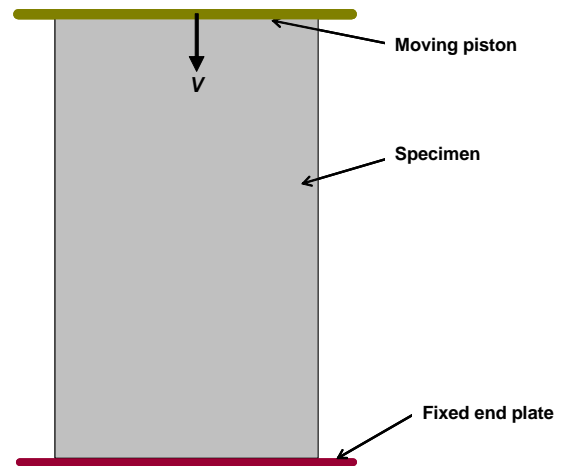


Figure 1: Uniaxial configuration with uniform velocity loading.

DIFFERENT LOADING CONDITIONS

In a uniaxial test, the load on the specimen is usually applied so as to produce a uniform strain rate. The movement of the piston is hydraulically controlled to

ensure that the loaded end is deformed at the required constant rate, thus causing a uniform longitudinal strain in the specimen. This is termed as ‘uniform velocity loading’, also known as ‘constant strain rate loading’. This type of loading is particularly suitable where the possibility of acceleration or deceleration of the loading piston can cause sudden fluctuation in the applied pressure. The motion of the piston at a specified constant rate prevents any accelerated motion and ensures a uniform rate of deformation of the loaded face of the specimen. Another common loading mechanism is ‘uniform pressure loading’, where a constant force is applied on the piston, which in turn is transmitted to the test specimen. This exerts a uniform pressure on the specimen at the loaded surface. In this work, we consider only the uniform velocity loading condition.

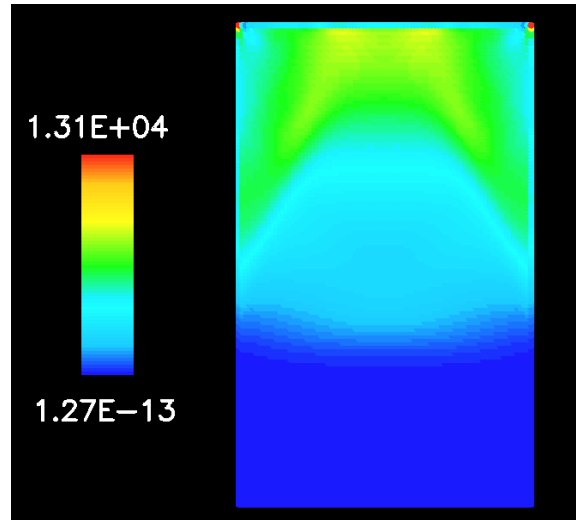
In this study we adopt von Mises stress (Timoshenko and Goodier, 1984) as the criterion (structural response) for analysing the stress field and elastic wave propagation in the specimen. The von Mises stress combines normal and shear components of the deviatoric stress tensor at a point, and is a commonly used criterion to assess failure (design) strength of materials.

Uniform Velocity Loading

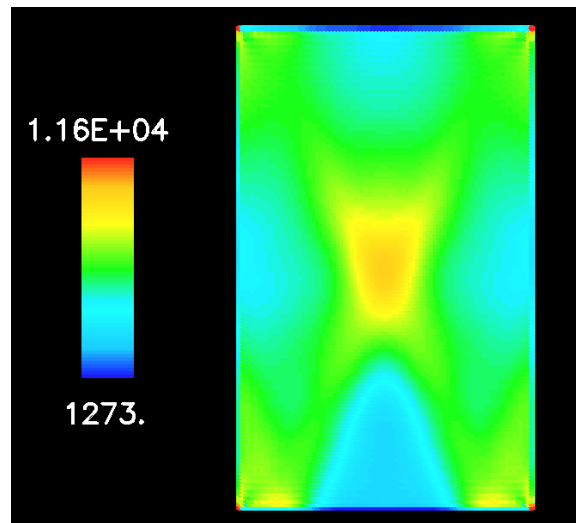
In this example the piston was moved vertically downwards at a constant velocity of 1.5 mm/s, while the bottom end of the specimen was kept fixed by placing it on a rigid plate, see Figure 1. In the initial stage of loading, we observe the transient phenomenon of elastic stress wave propagation within the specimen. This state will be termed as the ‘transient state’ in this paper. Figure 2 demonstrates the nature of wave propagation through the specimen. As a consequence of the current boundary conditions, the waves initiate from the top of the specimen and propagate downwards. The rapid variation in the stress pattern in the specimen is shown in Figure 2.

On reaching the bottom surface, the elastic waves reflect from the rigid plate at the bottom of the specimen. The reflected waves then propagate back upwards and interfere with the (newly generated) incident waves from the top (Figure 3). This creates a wave pattern by superposition of the incident waves and the reflected waves (from the bottom plate). The ‘superposed’ waves propagate further up through the specimen and are then reflected from the moving top piston. These reflected waves again interact with the waves reflected from the bottom plate. The superposition of the waves alternately reflected from the top piston and bottom plate continues. This phenomenon gradually leads to a complex interacting stress wave pattern in the specimen, as seen in Figure 3. The variation in the amplitude of the superposed elastic waves leads to spatial fluctuation in the von Mises stress distribution. The resulting stress variation is shown in Figure 3.

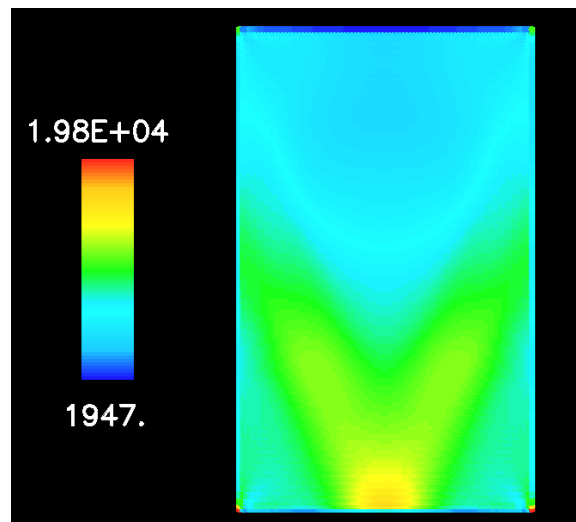
After sometime the interacting waves reach a steady state with little change in the stress wave pattern with time. However, the magnitude of the stresses at all points in the specimen continues to increase uniformly. As the top piston is being pushed vertically down, the specimen is compressed axially, which steadily increases the magnitude of the stress.



(a) $t = 0.04$ ms

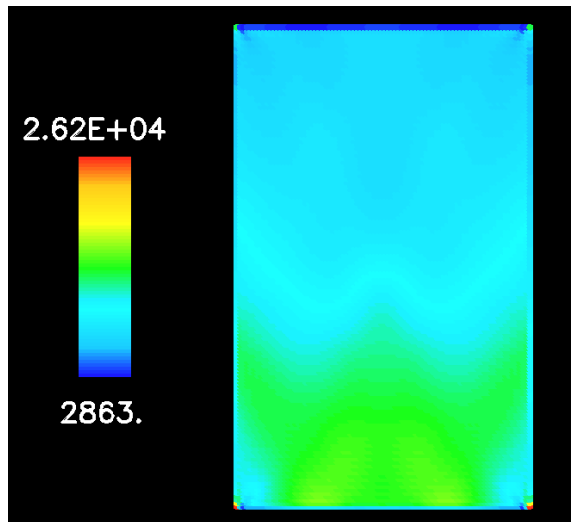


(b) $t = 0.08$ ms

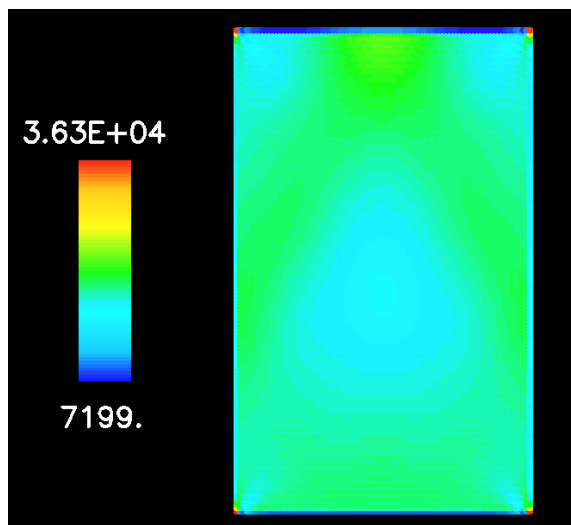


(c) $t = 0.11$ ms

Figure 2: Stress wave propagation from the top piston towards the bottom plate for uniform velocity loading case.



(a) $t = 0.12$ ms



(b) $t = 0.24$ ms

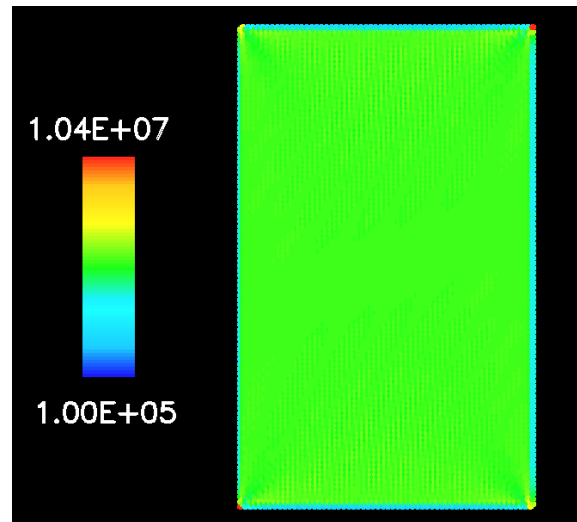
Figure 3: Reflected waves propagation from the bottom plate and their interaction with the waves originating from the top piston for uniform velocity loading case.

The steady state stress distribution is shown in Figure 4 and is extremely even. It may be noted that the corners of the specimen, due to the presence of sharp geometry changes, create regions of (theoretical) stress singularities. This induces and maintains ‘localised’ high stresses at the corners throughout the simulation, which is a physically intuitive phenomenon.

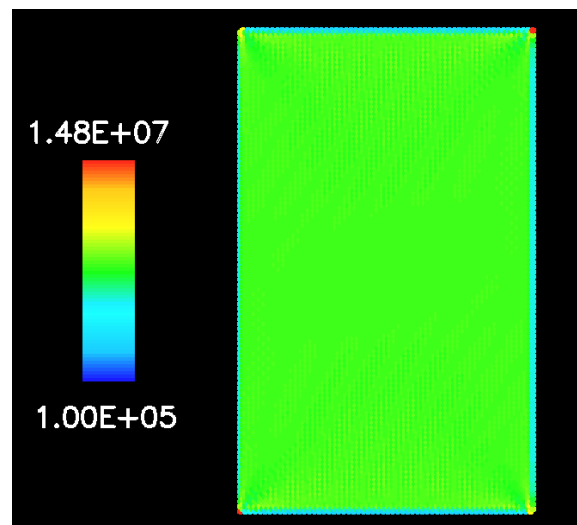
To monitor the stress variation, we select three representative points in the specimen, as shown in Figure 5. The rationale behind choosing these three specific points are:

- Point A (0 mm, 70 mm) lies on the vertical and horizontal planes of symmetry (planes v-v’ and h-h’).
- Point B (21.5 mm, 103.5 mm) lies on neither of the symmetry planes.
- Point C (21.5 mm, 70 mm) lies on a single symmetry plane (plane h-h’).

These representative locations characterise the stress variation taking into account the problem symmetry.



(a) $t = 70$ ms



(b) $t = 100$ ms

Figure 4: Steady state response of the specimen with little change in stress pattern for uniform velocity loading case.

The variation of the von Mises stress as the specimen is loaded is shown in Figures 6-8 for both the transient and steady responses. The instantaneous response of the structure when the load is just applied is shown in Figure 6 for a very short period of 0.1 ms. The stress at point B is raised first by the load (blue line in Figure 6). This is followed by rise in stress levels at points A and C, see Figure 6, as the initial stress wave reaches these locations. This is physically intuitive as point B is near the loading (top) edge. So the initial stress waves first reach point B and then points A and C. As points A and C are at same distance from the top edge, the rise in stress levels at these locations is observed almost simultaneously. After the instantaneous sharp rise and the initial oscillations in the stress levels, the subsequent transient stress pattern (up to ~3.5 ms) exhibits reduced waviness in stress variation. This is because the amplitude of the elastic waves diminishes rapidly and the response becomes approximately linear, reaching a steady state, see Figure 7.

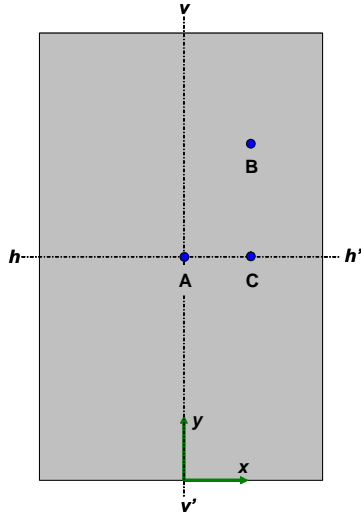


Figure 5: Locations of the representative points in the specimen for monitoring von Mises stress variation.

In a laboratory scale uniaxial test, our primary focus is the steady state response of the structure. Ideally, for a linear elastic structure the steady state response should consist of a uniform stress distribution at various locations (apart from the loading region where contact mechanics plays a dominant role and affects the local stress field). Once the system has reached steady state ($t > 3.5$ ms), the stresses at points A, B, and C are found to be the same at any given time and vary linearly with load (and therefore time). This demonstrates that the SPH method is producing the expected uniform (spatial) stress distribution at steady state and linear elastic structural behaviour (Figure 8).

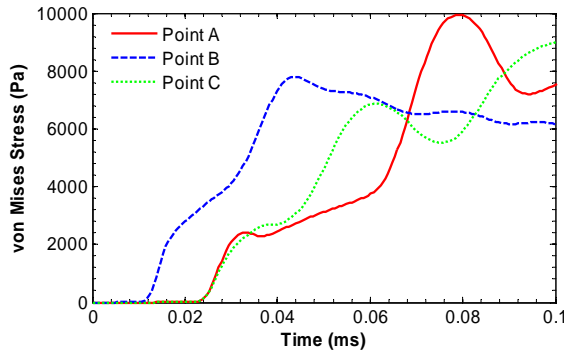


Figure 6: Very early stress variation in response to loading at the representative points.

FINITE ELEMENT ANALYSIS AND VALIDATION

The Finite Element Method was also used to model the uniaxial test so as to provide a high quality solution with which to compare the SPH solutions. The domain of the specimen was meshed with quadratic (8-node) reduced-integration quadrilateral elements. The finite element solution was obtained using an implicit dynamic analysis. The results presented in this section use a SPH particle resolution of 1 mm, which is the same as the element size used with the Finite Element Method. The mesh resolution with FE and the particle resolution with SPH were kept same so as to enable a comparative study of the two

methods using fundamentally different numerical concepts (used in FE and SPH). The effect of different particle resolutions on the SPH solutions and their comparison with the FE solution is reported in the later section.

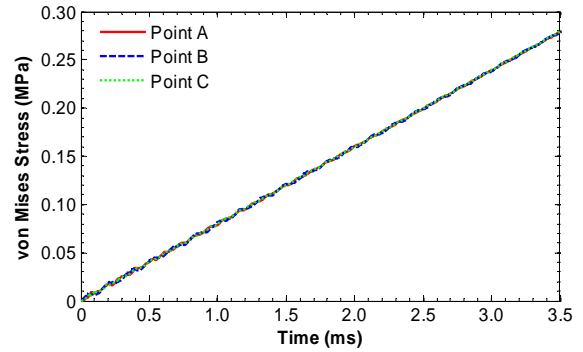


Figure 7: Stress variation at the three representative points in the specimen as a function of time (load) in the initial stage.

The same uniform velocity boundary condition of 1.5 mm/s (vertically downwards) was imposed on the top surface of the specimen. The bottom surface was again constrained to be fixed (as in Figure 1).

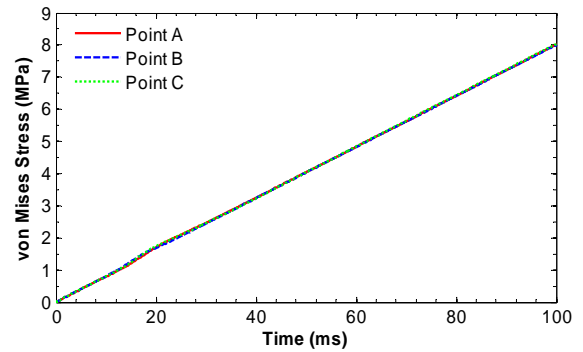


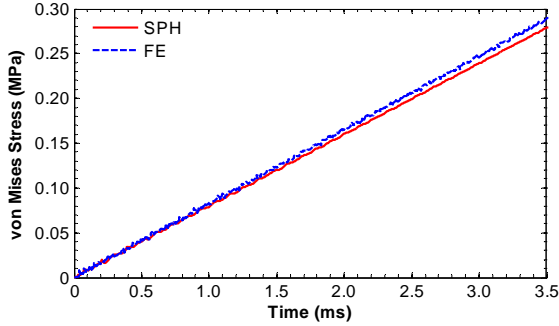
Figure 8: Stress variation at the three representative points in the specimen over longer times when the system has reached steady state.

The finite element solution was taken as the basis for evaluating the accuracy of the SPH method for stress analysis. Figure 9 shows the comparison between the SPH and the FEM predictions of the von Mises stress over time at point A (from Figure 5) in the specimen. The solutions agree very well for both the transient and steady state stages of compression. The maximum relative (%) deviations from the FE solutions were 4.9%, 5.5%, and 7.1% for points A, B, and C (in Figure 5) respectively. For the transient region the FE solutions have considerable oscillations (as seen in Figure 9(a)), whereas the SPH solutions are smooth and non-oscillatory, see Figure 9(a). This indicates that SPH solutions show more stability in capturing the initial transient response (elastic stress wave propagation) in the specimen.

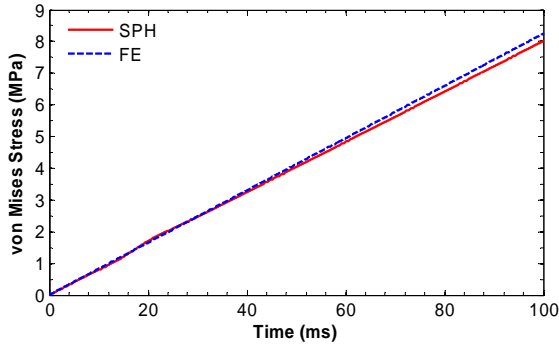
Effect of Particle Resolution on the Stress Field

The application of Smoothed Particle Hydrodynamics for structural stress analysis is relatively new. Hence, it is instructive to perform a convergence study to assess the effect of particle resolution on the SPH solution. The

uniaxial test was modelled with two more different particle resolutions (1.5 mm and 2 mm) in addition to the 1 mm resolution case reported so far. The stress field obtained for each particle resolution case was compared with the FE solution at each of the representative locations (points A, B and C in Figure 5). The results are presented in Figure 10 for point B. It can be seen that all the particle resolutions produce desired linear stress variation and show no instability.



(a) Transient state at point A



(b) Steady state at point A

Figure 9: Comparison of von Mises stress at point A in the specimen using SPH and FEM.

The relative difference between the SPH and the FE results are found to be SPH resolution dependent (as one should expect). A fine particle resolution leads to a solution closer to the corresponding finite element solution. For example, the deviation from the FE solution is illustrated in Figure 11 for point B in the steady state region. It can be observed that the difference grows gradually, reaches a limiting value, and then does not vary significantly. As expected, the coarser the particle resolutions, the higher the difference between the SPH and FE solutions. Furthermore, the relative difference between the SPH and FE solutions is found to be approximately proportional to the square of the particle resolution (Figure 11). This is consistent with the second order accuracy expected in a two dimensional problem domain. A detailed resolution study against an analytical solution or a numerical solution with a considerably fine mesh will appear in a later paper.

Gravity Loading

One load case was investigated to study the effect of gravity on the specimen. The purpose of this study is to assess the stability of the inherently transient SPH methodology to predict a steady state solution. The specimen was placed on a rigid platform under gravity only, and the von Mises stress field in the specimen was

monitored. This specific example was chosen as it is a simple problem with a static solution. The variation in the von Mises stress in the specimen is shown in Figure 12. Initially the stress levels reach to the static stress values (as determined by the gravity), and thereafter the stress levels remain essentially the same. The magnitude of the stresses at various points depends on their distances from the reference horizontal plane (i.e. the bottom surface of the specimen). This is evident from the graded stress pattern in Figure 12. Furthermore, the solution is found to stabilise rapidly. This demonstrates the stability of the current SPH implementation in predicting steady state solutions.

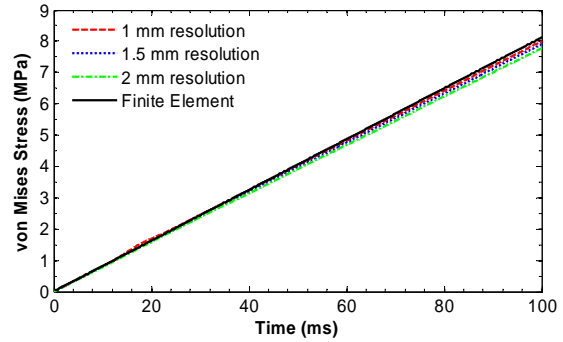


Figure 10: Steady state stress variation at point B for different SPH particle resolutions and their comparison with the finite element solution.

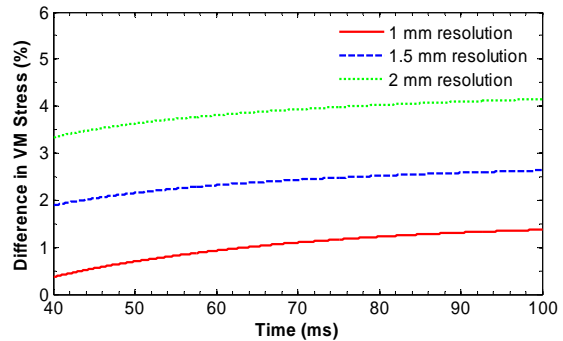


Figure 11: Deviation of von Mises stress from the finite element solution at point B for different SPH particle resolutions.

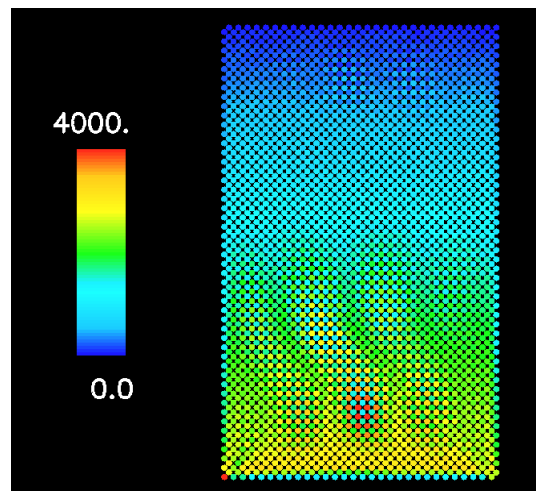


Figure 12: von Mises stress distribution in the specimen at $t = 60$ ms subjected to gravity loading.

DISCUSSION

This work demonstrates that Smoothed Particle Hydrodynamics is able to accurately predict stress wave propagation and material deformation in uniaxial compression tests on laboratory scale specimens. The boundary conditions on the specimen can be imposed in a variety of ways, such as velocity based loading, pressure based loading, and gravity loading. The effect of varying test parameters on specimens of various dimensions and materials can be rapidly assessed by the SPH technique as pre-processing (meshing and boundary conditions) requirements with SPH is considerably less than those needed with conventional mesh-based techniques, and SPH can produce good accuracy with a (relative to FE) coarser resolution.

In the current SPH implementation, the loading piston and the fixed jaw (plate) are explicitly modelled, and the loads and constraints are applied through them. Therefore in the present application of SPH, the boundary conditions are imposed by modelling the realistic loading or constraining agents explicitly, such as the loading piston and the fixed plate here. This direct contact modelling simulates realistic test conditions better than simulated using specified boundary conditions (uniform pressure or velocity), which are commonly used with the Finite Element Method. Indeed, when using FEM, the simulation of contact between the surfaces (e.g. piston and specimen here) involves detailed pre-processing requirements for accurate contact definition and very fine mesh to capture the interactions between the surfaces in contact. With SPH the modelling of contact for the purpose of normal load transmission can be performed without resolving complex aspects of detailed contact mechanisms and without requiring a finely graded mesh near the load boundaries (as needed in the Finite Element Method). This is particularly advantageous when simulating mechanical tests that involve surfaces transmitting normal loads. The typical uniaxial test problem was also analysed using the Finite Element Method. It was found that the response of the specimen obtained using SPH agreed very well with the finite element solution.

CONCLUSIONS

This study has evaluated and established Smoothed Particle Hydrodynamics as an effective and efficient numerical tool for stress analysis, modelling elastic stress wave propagation and simulating mechanical tests. The generation, reflection and superposition of the elastic waves are well captured using SPH. The SPH solutions can predict attainment of steady state conditions and show no instability. The stable response under gravity loading illustrates the ability of SPH in modelling static stress analysis problems. The proper load transfer to the specimen indicates that an SPH based approach can be used for simulating realistic test conditions involving a variety of load cases. Moreover, the SPH formulation used here can provide accuracy comparable to that of FEM. This will enable rapid analysis of a wide range of test scenarios.

This study has also established the potential strengths of SPH as a numerical tool that can be used for modelling fracture in compression tests. The SPH solution matches the FE result for non-fracturing cases in accuracy and can

easily handle the discontinuous large scale deformation involved in fracture problems due to its mesh-less nature. Furthermore, the Lagrangian formulation makes SPH well suited to simulating damage initiation and propagation by tracking the history of stress-strain state of the particles. Therefore, the underlying numerical concepts and formulations embedded in Smoothed Particle Hydrodynamics provide an effective framework for modelling fracture problems.

REFERENCES

- ALIABADI, M. H. and ROOKE, D. P., (1991), "Numerical Fracture Mechanics": Computational Mechanics Publications and Kluwer Academic Publishers.
- BRADLEY, G. L., CHANG, P. C. and MCKENNA, G. B., (2001), "Rubber modeling using uniaxial test data", *Journal of Applied Polymer Science*, **81**, (4), 837-848.
- CLEARY, P. W., PRAKASH, M. and HA, J., (2006), "Novel applications of smoothed particle hydrodynamics (SPH) in metal forming", *Journal of Materials Processing Technology*, **177**, (1-3), 41-48.
- CLEARY, P. W., PRAKASH, M., HA, J., STOKES, N. and SCOTT, C., (2005), "Smooth Particle Hydrodynamics; Status and future potential", In *Proc. 4th International Conference on CFD in the Oil and Gas, Metallurgical & Process Industries*, Norway. ed. S. T. Johansen.
- FERNANDEZ-MENDEZ, S., BONET, J. and HUERTA, A., (2005), "Continuous blending of SPH with finite elements", *Computers and Structures*, **83**, 1448-1458.
- GRAY, J. P., MONAGHAN, J. J. and SWIFT, R. P., (2001), "SPH elastic dynamics", *Computer Methods in Applied Mechanics and Engineering*, **190**, (49-50), 6641-6662.
- LI, S.-H. and WANG, Y.-N., (2004), "Stochastic model and numerical simulation of uniaxial loading test for rock and soil blending by 3D-DEM", *Yantu Gongcheng Xuebao/Chinese Journal of Geotechnical Engineering*, **26**, (2), 172.
- LIBERSKY, L. D. and PETSCHKE, A. G., (1990), "Smooth particle hydrodynamics with strength of materials", In *Advances in the Free-Lagrange Method*, ed. T. a. Crowley, Berlin: Springer.
- MONAGHAN, J. J., (1992), "Smoothed particle hydrodynamics", *Ann. Rev. Astron. Astrophys.*, **30**, 543-574.
- NAWROCKI, P. A., DUSSEAULT, M. B. and BRATLI, R. K., (1998), "Use of uniaxial compression test results in stress modelling around openings in nonlinear geomaterials", *Journal of Petroleum Science & Engineering*, **21**, (1-2), 79-94.
- TIMOSHENKO, S. and GOODIER, J. N., (1984), "Theory of elasticity", 3rd ed. McGraw-Hill.
- WINGATE, C. A. and FISHER, H. N., 1993. Strength Modeling in SPHC. *Los Alamos National Laboratory*, Report No. LA-UR-93-3942.